Lagrangian chaos, Eulerian chaos, and mixing enhancement in converging–diverging channel flow

Cristina H. Amon,[a] Amador M. Guzmán,[a] and Benoit Morel[b]
Carnegie Mellon University, Pittsburgh, Pennsylvania 15213

(Received 18 July 1995; accepted 22 January 1996)

A study of Lagrangian chaos, Eulerian chaos, and mixing enhancement in converging–diverging channel flows, using spectral element direct numerical simulations, is presented. The time-dependent, incompressible Navier–Stokes and continuity equations are solved for laminar, transitional, and chaotic flow regimes for $100 \leqslant Re \leqslant 850$. Classical fluid dynamics representations and dynamical system techniques characterize Eulerian flows, whereas Lagrangian trajectories and finite-time Lagrangian Lyapunov exponents identify Lagrangian chaotic flow regimes and quantify mixing enhancement. Classical representations demonstrate that the flow evolution to an aperiodic chaotic regime occurs through a sequence of instabilities, leading to three successive supercritical Hopf bifurcations. Poincaré sections and Eulerian Lyapunov exponent evaluations verify the first Hopf bifurcation at $125 < Re < 150$ and the onset of Eulerian chaos at $Re \approx 550$. Lagrangian trajectories and finite-time Lagrangian Lyapunov exponents reveal the onset of Lagrangian chaos, its relation with the appearance of the first Hopf bifurcation, the interplay between Lagrangian and Eulerian chaos, and the coexistence of Lagrangian chaotic flows with Eulerian nonchaotic velocity fields. Last, Lagrangian and Eulerian Lyapunov exponents are used to demonstrate that the onset of Eulerian chaos coincides with the spreading of a strong Lagrangian chaotic regime from the vortex region to the whole fluid domain. © *1996 American Institute of Physics.*
[S1070-6631(96)01205-6]

I. INTRODUCTION

Chaos is a phenomenon that has been found in many physical systems and has been confirmed both theoretically and experimentally. Manifestations of chaos involve a wide range of mechanical, electrical, and optical systems, hydrodynamic processes of various length scales, transport processes and chemical reactions, neurophysiological processes, ecological and urban systems, and celestial mechanics.

One important application where chaos theory has been shown to be beneficial is in the understanding and exploitation of fluid mixing.[1] Regular convective mixing due to vortices, recirculation regions, or cellular convection enhances heat transfer by increasing the fluid advection. One characteristic of this kind of mixing is that particle paths are nonchaotic, that is, trajectories of neighboring particles remain relatively close to each other. When conditions are such that particle paths are chaotic, there occurs an additional increase in heat transfer derived from the random motion of the fluid particles. A similar increase is observed for turbulent flows in which turbulent mixing is responsible for high rates of heat transport. However, any kind of mixing is also accompanied by transverse momentum transfer, leading to higher wall shear stresses and requiring more mechanical power to maintain a given flow rate.

A. Eulerian and Lagrangian chaos

The hydrodynamic equations of motion can be studied following two different approaches known as Eulerian and Lagrangian. In the Eulerian approach, the velocity and pressure fields are solved in the spatial domain at any time. From a dissipative system theory viewpoint, trajectories in the phase space move around an attractor, which can be periodic, quasiperiodic, or strange, depending on the control parameter of the flow. Thus, *Eulerian chaos*, also named turbulence, can be interpreted as the state of a system in a strange attractor with at least one positive Lyapunov exponent.[2,3] In the Lagrangian approach, we deal with the trajectory of each fluid particle. If $\mathbf{u}(\mathbf{x},t)$ denotes the Eulerian velocity field, the motion of a fluid particle initially located at $\mathbf{x}_0=\mathbf{x}(t_0)$ is then determined by the differential equation $d\mathbf{x}/dt=\mathbf{u}(\mathbf{x},t)$. Thus, a state of *Lagrangian chaos*, sometimes referred to as chaos, can be recognized when the solution of the trajectory equations has a sensitive dependence on initial conditions, and initially nearby trajectories diverge exponentially fast.[3,4] In Lagrangian chaos, the phase space is conservative, thereby attractors are nonexistent. The possibility of having Lagrangian chaos without Eulerian chaos indicates that mixing enhancement does not require Eulerian chaos. In this paper, Eulerian may be referring to weak turbulence and Lagrangian chaos refers to chaos.

Even though various researchers have investigated the relation between Lagrangian and Eulerian chaos, a general and unique relationship has not yet been found.[3–6] Lagrangian and Eulerian chaotic states can be identified by calculating the Lagrangian and Eulerian Lyapunov exponents, λ_L and λ_E, respectively, which do not seem to be simply related. Results obtained in truncated models of the Navier–Stokes equations[4] show that λ_L is not affected by sharp increases of λ_E at the critical Reynolds number. These results provide numerical evidence that the onset of Eulerian chaos cannot be predicted from Lagrangian flow characteristics. In addition, a chaotic velocity field generally implies a chaotic mo-

[a]Mechanical Engineering, APS members.
[b]Physics and Engineering & Public Policy, APS member.

 1070-6631/96/8(5)/1192/15/

tion of particles, with the exception of the Lorenz model[7] and the chaotic motion in the point vortex model,[5] which exhibit Eulerian chaos without Lagrangian chaos. One question that arises here is whether Lagrangian chaos implies an enhancement of mixing. Next, we review previous research on chaotic advection and mixing.

B. Chaotic advection and mixing

Mixing is directly related to the motion of fluid particles and is a central issue in heat and mass transfer processes. The enhancement of mixing due to Lagrangian chaos is referred to as chaotic advection. Most of the work on chaotic advection has focused on simple geometry flow regimes. Researchers have found that two-dimensional time-periodic flows generate complex trajectories of test particles in a Lagrangian framework.[8–14] The chaotic advection phenomenon of a stirred tank flow was studied by modeling the agitator as a point vortex and assuming incompressible, inviscid two-dimensional flows.[8] The motion of a particle shows that an unsteady blinking vortex causes more rapid mixing and fluid stretching than a single fixed vortex. Sobey[9] simulated numerically the motion of fluid tracer particles in an external pulsating furrowed channel flow to study dispersion phenomenon and mixing processes. Increases in mixing for eccentric journal bearing flows and for driven cavity flows have been observed by Chaiken *et al.*[10] and Chien *et al.*,[11] respectively. Howes *et al.*[12] studied flow mixing enhancement in a baffled channel by the superposition of a time-periodic flow on a steady flow. By using numerically generated flow visualizations, they observed a regime of chaotic advection for unsteady flows. They also found that the combination of periodic baffles and unsteady flow regimes resulted in good radial mixing. Perkins *et al.*[13] investigated mixing enhancement and heat transfer augmentation through a channel containing periodic square obstructions. Tangborn *et al.*[14] studied the chaotic advection in a two-dimensional mixed-convection flow and determined that Lagrangian motion of fluid particles becomes chaotic right after reaching the critical Reynolds number for periodic flow, that is, at the onset of unsteadiness of the Eulerian velocity field. However, calculations of the effect of Lagrangian chaotic motion on the mixing efficiency were not reported. Solomon and Gollub[15] studied the chaotic particle transport in time-periodic Rayleigh–Bénard convection and found that the basic transport mechanism is chaotic advection in the vicinity of oscillatory roll boundaries. Shariff *et al.*[16] studied numerically the kinematics of fluid elements for a flow past a circular cylinder in the regime of time-periodic vortex shedding. Based on stable and unstable manifolds, they found that the stretch of fluid elements tends to be larger close to the unstable manifolds. The efficiency of mixing is, to a large extent, determined by the *stretching rate*,[17] which is directly related to the Lagrangian Lyapunov exponent, λ_L. The Lagrangian Lyapunov exponent is by definition the time average of the stretching rates. Consequently, we can interpret the stretching distributions as finite-time Lagrangian Lyapunov exponent distributions.

II. ANALYTICAL STUDIES ON LAGRANGIAN AND EULERIAN CHAOS

In this section we discuss recent studies on Lagrangian and Eulerian chaos[3,5,6] and describe the actual knowledge on the relationship between Lagrangian and Eulerian chaos. These previous studies, limited to simple geometries where the use of analytical tools is appropriate, show that even though advances have been made, we are far from having a thorough understanding of the relationship between Lagrangian and Eulerian chaos. This is more so when realistic engineering devices are considered, since traditional analytical tools, based mostly on evolution equations, are neither applicable nor available.

There are two different approaches to producing and describing stochastic particle motions in a fluid, as pointed out by Aref.[18] In the first approach, individual particles in a given system move according to stochastic equations of motion (e.g., advection in a turbulent flow). In the second approach, the stochastic particle motion arises from a flow field described by deterministic equations of motion (e.g., chaotic advection). The connection between chaotic advection due to Lagrangian chaos and turbulence related to Eulerian chaos is still unclear. Most studies on chaotic advection have been performed using analytical tools derivated from dynamical system theory. The velocity field is either obtained from a streamfunction or expressed as a nonautonomous system of ordinary differential equations (ODEs) that satisfies governing equations and boundary conditions, or based on systems with singularities such as point vortices. In analytical studies of chaotic advection, the Eulerian velocity field is either steady or time periodic. In the former, a time-periodic infinitesimal perturbation is added to the steady flow. Thus, the new ODE governing the fluid motion can exhibit Lagrangian chaos but the Eulerian perturbed velocity field is itself time periodic.

Rom-Kedar *et al.*[6] studied fluid particle motions in a velocity field induced by two oscillating counter-rotating point vortices of equal strength, subject to a sinusoidal time-periodic strain field. They used the explicit connection between particle motions in a two-dimensional incompressible flow and a two-dimensional Hamiltonian dynamical system. Since it involves only kinematic considerations, the results are independent of the Reynolds number. The analysis of the flow topology is based on two concepts introduced by the authors: (a) the *tangle dynamics*, i.e., the behavior of stable and unstable manifolds as a partial barrier of transport and the intersection between the manifolds that influences the stretching and deformation of fluid elements; and (b) the *finite time stretch*, i.e., the temporary exponential stretching of particle trajectories undergoing chaotic motion and finite time interval over which most of this stretching takes place. The latter concept is important in open flows, where fluid particles spend only a finite time on a chaotic zone. The stable and unstable manifolds coincide with each other for unperturbed flows. However, the stable and unstable manifolds intersect transversally in the perturbed flow forming a tangle, and nearby fluid particles may separate at an exponential rate yielding chaotic fluid particle motion. The existence of transverse heteroclinic orbits, determined by using

the Melnikov function method, gives rise to Smale horseshoes as a result of stretching and folding—the mechanism for chaotic particle motion.

Danielson and Ottino[3] investigated a two-dimensional wall flow based on a separation bubble near the wall that reveals a topological similarity to a heteroclinic orbit. They use a method for constructing flows that involves asymptotic expansions from a point located at the wall. They obtain an ODE system by considering a fifth-order expansion and enforcing the series to satisfy the governing equations and nonslip boundary conditions at the wall. Specific topological characteristics of a separation bubble, such as separation and attachment points, are considered to close the system of ODEs. Their results demonstrate that the flow undergoes a bifurcation to a time-periodic solution and that this bifurcation provides an adequate periodic perturbation to the heteroclinic orbit represented by the separation bubble, inducing chaotic advection. The existence of Lagrangian chaos is demonstrated by representing the intersection of stable and unstable manifolds. The broadband nature of the Fourier power spectra for a fixed spatial location and the evolution to a strange attractor via a period-doubling route indicates a regime of Eulerian chaos.

Babiano *et al.*[5] studied the motion of passively advected particles in a velocity field generated by three- and four-point vortices in an infinite domain described by a time-periodic streamfunction. To investigate regular and chaotic behaviors, they obtain Lagrangian trajectories of fluid particles in different regions of the vortices and Eulerian motion of the vortices. They found that particle trajectories may be chaotic, even for a regular velocity field with a vanishing Eulerian Lyapunov exponent. A point vortex that presents a chaotic motion is surrounded by an island where advected particles perform a regular orbit with a zero Lagrangian Lyapunov exponent. However, passive particles far from the vortices, but between them, present a chaotic motion with a positive Lagrangian Laypunov exponent. They obtain a similar result for passive particles located in a complex two-dimensional turbulent Eulerian flow formed by four-point vortices of constant and similar size.

Based on these previous studies, a generalization of chaotic advection and of the relationship between Lagrangian and Eulerian chaos is not possible. In realistic engineering devices of finite length and variable geometry, the vortex dynamics is more complex. The converging–diverging open flow system[25] with more complicated vortical structures can be seen as a generalization of the system analyzed by Rom-Kedar *et al.*[6] The flow is symmetric until the first Hopf bifurcation appears, and further increases in the Reynolds number leads to an asymmetric flow. Since analytical expressions of the velocity field based on streamfunctions are not known, we perform direct numerical simulations (DNS) of the time-dependent Navier–Stokes equations to obtain the Eulerian velocity field. Therefore, no explicit evolution equations are available for the Lagrangian flow, and we obtain the Lagrangian trajectories by numerical integration of the Eulerian velocity field.

According to Aref,[18] a sufficient condition for mixing is to involve as many particles as possible in motions that are

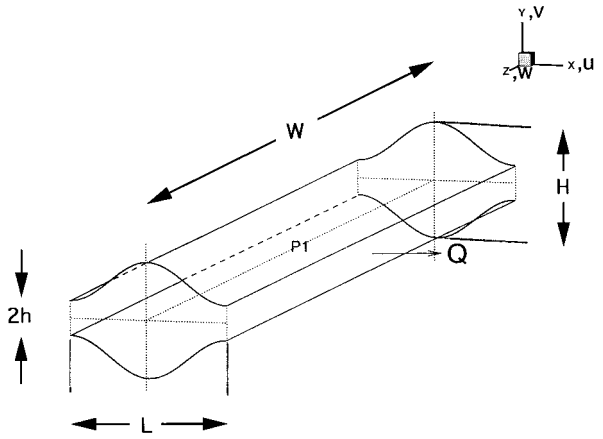

FIG. 1. Converging–diverging channel: nondimensionalized periodicity length $L/h=9.33$, spanwise length $W/h=53.33$, and maximum height $H/h=6.66$. P1: $(x/h,y/h,z/h)=(4.67,3.33,26.67)$.

stochastic. Then a mathematical description of fluid mixing must address the production and characterization of stochastic motions of fluid particles. In the analytical study of an oscillating pair of vortices, Rom-Kedar *et al.*[6] identify three zones: the free flow region, the core, and the mixing region. The mechanism of fluid transfer between the vicinity of the core and the free flow region is based on the splitting of both the stable and unstable manifolds, so the region bounded by the envelope of the manifolds is called the mixing region and the resulting structure is known as the stochastic layer. Heteroclinic trajectories, unstable manifolds, edge of vortices, and stochastic layers are concepts borrowed from Hamiltonian dynamical system and used for describing and quantifying chaotic motions of fluid particles and mixing. One of the long-term goals of this study is to investigate the possibility to achieve high heat transfer rates in transitional flows in converging–diverging channels without the penalty associated with the significant increase of pumping power in turbulent flows. Thus, we investigate whether mixing enhancement by chaotic flow advection would lead to significant heat transfer enhancement on nonchaotic Eulerian flows. To address this, we evaluate the mixing enhancement by calculating first the distribution of finite-time Lagrangian Lyapunov exponents of fluid elements in the vortical regions. Future work will relate heat transfer enhancement to the evolution of the tail of the distribution of finite-time Lagrangian Lyapunov exponents.

III. PHYSICAL PROBLEM

The converging–diverging channel shown in Fig. 1 is a symmetric wavy-walled channel employed for enhancing heat and mass transfer efficiency of industrial transport processes. It is also used in biomedical applications such as a membrane oxygenator and kidney dialyzer for the purpose of enhancing mass transfer rates. Numerical calculations and experimental studies have been performed in converging–diverging channels, and global flow patterns have been reported.[19–24] For low Reynolds numbers there is a stagnant flow region in the upstream part of each furrow. As the Reynolds number increases, recirculation zones appear on the

upper and lower furrows, with a flow symmetric with respect to the central line of the channel. As the Reynolds number increases further, the vortex center in each furrow of the channel moves downstream and the flow remains symmetric. Last, the flow becomes unsteady for larger Reynolds numbers and a mixing region with the mainstream is identified. These previous studies have only considered fully developed steady flows and pulsating external flows. Guzmán and Amon[25] investigated the onset and transition process to chaos by direct numerical simulations (DNS) of the Navier–Stokes equations in the converging–diverging channel flow. Their numerical results were based on classical fluid dynamical representations, such as time series, Fourier power spectra, and phase space portraits. These results reveal that the flow follows a sequence of three supercritical Hopf bifurcations as the Reynolds number increases from a laminar to a transitional regime, and that the transition to an Eulerian aperiodic chaotic flow occurs through the Ruelle–Takens–Newhouse scenario. The Reynolds number is defined as $\mathrm{Re}=\frac{3}{2}\cdot Uh/\nu$, where U is the average velocity, h is the half-height of the channel, and ν is the kinematic viscosity.

In this paper we report the dynamical characterization of laminar, transitional, and chaotic flow regimes using Lagrangian and Eulerian descriptions, and is a continuation of our previous paper on converging–diverging channel flows.[25] In this paper, we characterize the strength and dynamical properties of chaotic flow regimes by DNS of the governing equations. We determine the predictability of transitional and weak turbulent flows. We confirm the evolutive flow pattern and the sequence of bifurcations in the transition to Eulerian chaos found in converging–diverging channel flows by means of classical fluid dynamic representations.[25] Through the Lagrangian characterization of these flow regimes, we investigate the onset of Lagrangian chaos and its relation to the first flow instability of the Eulerian velocity field. We quantify the strength of Lagrangian chaotic regimes, its relation to the onset of Eulerian chaos and the mixing improvement due to chaotic advection. Last, we investigate the relationship between Lagrangian and Eulerian chaos in converging–diverging channel flows. We use the spectral element method[25–27] to solve the governing Navier–Stokes and continuity equations and to obtain the Eulerian velocity and pressure fields. Because the velocity field is obtained by DNS, no analytical, time-continuous evolution equations are available to relate the Eulerian velocity at fixed points with Lagrangian positions of fluid particles. The Lagrangian trajectories of fluid particles are obtained therefore by numerical integration of the Eulerian velocity field in the whole computational domain. Details of the mathematical formulation, the numerical approach, and the algorithms are given in Sec. IV.

The remainder of this paper is organized as follows: In Sec. IV, we outline the mathematical formulation and discuss the numerical algorithms to perform the computational simulations. In Sec. V, we present the results of the direct numerical flow simulations for the Eulerian and Lagrangian characterizations. Then, in Sec. VI, we discuss the Eulerian and Lagrangian representation results, and last, in Sec. VII, we summarize this investigation.

IV. PROBLEM FORMULATION AND ALGORITHMS

Numerical investigations on the periodically converging–diverging channel flows are performed by Direct Numerical Simulations of the time-dependent, two-dimensional, incompressible Navier–Stokes and continuity equations, given by

$$\frac{\partial \mathbf{v}}{\partial t}=\mathbf{v}\times\boldsymbol{\omega}-\boldsymbol{\nabla}\pi+\frac{1}{\mathrm{Re}}\nabla^2\mathbf{v}, \tag{1}$$

$$\boldsymbol{\nabla}\cdot\mathbf{v}=0, \tag{2}$$

where $\mathbf{v}$ is the Eulerian velocity field; $\pi=p+\frac{1}{2}\mathbf{v}\cdot\mathbf{v}$ is the dynamic pressure; $\boldsymbol{\omega}=\boldsymbol{\nabla}\times\mathbf{v}$ is the vorticity; and Re is the Reynolds number. The flow is fully developed in the streamwise x direction and homogeneous in the spanwise z direction (Fig. 1). The boundary conditions are nonslip at the walls and periodicity of the fully developed flow in the x direction.

The governing equations (1)–(2) subject to the boundary conditions are solved numerically using a spectral element method.[26,27] A three-step, time splitting scheme for the semi-discrete formulation of the time-dependent term in the Navier–Stokes equations is employed. This splitting scheme consists of first, a nonlinear step for the convective term using an explicit third-order forward-in-time Adams–Bashforth scheme; second, a pressure step using an implicit Euler–Backward scheme for the pressure term and enforcing the incompressibility constraint; and finally, a viscous step employing an implicit Crank–Nicolson scheme, which includes the viscous correction and imposes the boundary conditions. For the spatial discretization in this spectral element method, the domain is first divided into quadrilateral macroelements, which are isoparametrically mapped from the physical space into the local coordinate system. Then the geometry, velocity, and pressure in each macroelement is represented as a tensor product of high-order Lagrangian interpolants through Gauss–Lobatto–Chebyshev collocation points. The nonlinear convective term is evaluated pseudospectrally, whereas the pressure and viscous terms, which correspond to modified Helmholtz equations, are solved by a variational approach.[26] The numerical results are obtained by direct simulation of the governing equations integrating in time, starting with a predicted steady flow and gradually increasing the Reynolds number until a steady, time periodic, or transitional flow is obtained. The temporal accuracy, the adequacy of the mesh, and the spatial discretization were analyzed and discussed in our previous paper on this converging–diverging channel.[25]

A. Dynamical system algorithms

To characterize laminar, transitional, and chaotic flow regimes from the Eulerian viewpoint, we use modern dynamical system techniques such as Poincaré section representations and Eulerian Lyapunov exponents. The Poincaré section method allows a systematic reduction in problem complexity by means of reducing the number of dimensions and converting a continuous-time evolution into a discrete-time mapping. For example, a seemingly complicated trajectory in a three-dimensional phase space can be depicted as a

Poincaré section representation, which exhibits a trajectory inscribed on a T^2 torus.[17,28] Poincaré sections have the same kind of topological properties as the flow from which they arise. Starting from observations of a signal $x(t)$, we reconstruct the topology of the attractor by taking the phase space $x(t)$, $x(t+\tau)$, $x(t+2\tau)$, and considering $x(t)$ independent of $x(t+\tau)$ and $x(t+2\tau)$, where τ is the time delay. This does not mean that the attractor obtained in the new space is identical to the original phase space; however, the new representation of the attractor retains the same topological properties. To build the Poincaré sections, we construct a state vector $F(t_s)=\{u(t_s),u(t_s+\tau)\}$ based on the time delay reconstruction, where t_s and τ are the sampling time and the time delay, respectively.[29] Then, we obtain a trajectory of the continuous-time evolution, defined by the state vector and the sampling time, such that each point of that trajectory is given by $\{u(t_s),u(t_s+\tau),t_s\}$. Last, the Poincaré section is determined by successive intersection points between this trajectory and a plane perpendicular to the time axis, at intervals of time T, where T is the period associated with the first fundamental frequency of the flow.

The Eulerian Lyapunov exponents spectrum, $\{\lambda_E\}$, provides a good characterization of the attractor geometric properties and of the dynamical flow properties. The Lyapunov exponent measures the long-time average exponential growth or decay of infinitesimal perturbations to a phase space trajectory, i.e., λ_E measures the sensitivity of the system to changes in initial conditions on the phase space. An attractor in an N-dimensional phase space has N Lyapunov exponents. If an attractor has one or more positive Lyapunov exponents, λ_E, perturbations on the attractor can grow exponentially fast in the directions of the positive exponents. In such a case, the attractor is chaotic and is called a *strange attractor*.[28] A negative λ_E implies an exponential decay toward the attractor.

B. Lagrangian description algorithms

The Lagrangian characterization of laminar and transitional flow regimes is based on Lagrangian trajectories of test particles $\mathbf{x}(t)$ that are obtained by direct numerical integration of the Eulerian velocity field, $\mathbf{u}(\mathbf{x},t)$, in the computational domain for any spatial location. The integration algorithm is as follows: (i) define the position of a fluid particle at a given time t_0 as $\mathbf{x}_0=\mathbf{x}(t_0)$ and get the velocity of this particle from DNS as $\mathbf{u}(\mathbf{x}_0,t_0)$; (ii) calculate the position of this fluid particle at time $t_1=t_0+dt$ as $\mathbf{x}_1=\mathbf{x}_1(t_1)=\mathbf{x}_0+\int_{t_0}^{t_1}\mathbf{u}(\mathbf{x}_0,t_0)\cdot dt$, where dt is a sufficiently small incremental time. The velocity of the fluid particle at the position $\mathbf{x}_1(t_1)$, $\mathbf{u}(\mathbf{x}_1,t_1)$, is calculated by high-order Lagrangian interpolation as $\mathbf{u}(\mathbf{x}_1,t_1)=\Sigma_i^N\Sigma_j^N\mathbf{u}_{ij}[x_{ij}(t_1),t_1]\cdot h_i h_j$, where $\mathbf{u}_{ij}[x_{ij}(t_1),t_1]$ are the Eulerian velocities calculated by DNS at the nodal points x_{ij} that are surrounding the position $\mathbf{x}_1(t_1)$, and $h_i h_j$ are high-order Lagrangian interpolants; (iii) calculate the new positions at successive times $t_n=t_{n-1}+dt$ as $\mathbf{x}_n=\mathbf{x}_{n-1}+\int_{t_{n-1}}^{t_n}\mathbf{u}(\mathbf{x}_{n-1},t_{n-1})\cdot dt$ until the final time is reached. The Lagrangian trajectory of the fluid particles is the set composed by the points $\{\mathbf{x}_0,\mathbf{x}_1,\mathbf{x}_2,...,\mathbf{x}_n\}$.

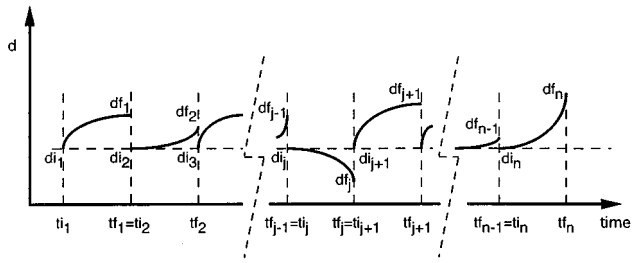

FIG. 2. Schematic representation of the algorithm to calculate the average finite-time Lagrangian Lyapunov exponent based on the convergency of initially nearby fluid particle trajectories.

Lagrangian chaos is a property of the dynamical system $d\mathbf{x}/dt=\mathbf{u}(\mathbf{x},t)$, whose solution $\mathbf{x}(t)$, calculated as described above, has a sensitive dependence on initial conditions. Therefore, trajectories initially nearby diverge exponentially fast. The Lagrangian Lyapunov exponent, λ_L, estimates the rate at which the distance between two fluid test particles, initially close, increases or decreases with time. Lagrangian chaotic regimes could occur in laminar and transitional flow regimes in the presence of well-organized Eulerian velocity fields. It induces mixing enhancement by chaotic advection and produces, in some devices, significant increases in the heat transfer performance with less cost in power input. In nonchaotic Lagrangian flow regimes, Lagrangian trajectories coincide with streamlines, whereas in Lagrangian and Eulerian chaotic flow regimes test particles follow complex Lagrangian trajectories.

The finite-time Lagrangian Lyapunov exponent, λ_L, is defined as

$$\lambda_L=\frac{1}{n}\sum_{j=1}^{n}\lambda_j,\quad \lambda_j=\frac{1}{tf_j-ti_j}\log_2\left(\frac{df_j}{di_j}\right),$$

where $di_j=|\mathbf{x}_p(ti_j)-\mathbf{x}_q(ti_j)|$ is the initial distance between two fluid particles p and q at the initial time ti_j, and df_j is the distance between the same fluid particles at time tf_j. The number n indicates the number of times that this operation is repeated for a continuous time evolution of the Eulerian velocity field. The sum of all λ_j gives the average finite-time Lagrangian Lyapunov exponent, λ_L, which represents the divergence (or convergence) of two initially nearby fluid particle trajectories. Figure 2 shows a schematic representation of the algorithm described above on a continuous finite-time evolution $(tf_1-ti_1)=(tf_2-ti_2)=\cdots=(tf_n=ti_n)$. This representation indicates that $di_1=di_2=\cdots=di_j=di_{j+1}=\cdots=di_n$ and, at times, $tf_j=ti_{j+1}$, $j=1,\ldots,n-1$, the fluid particles p and q are positioned again at the initial positions $\mathbf{x}_p(ti_j)$ and $\mathbf{x}_q(ti_j)$, respectively. Therefore, these two fluid particles, p and q, remain most of the time confined to the vortex region or the region in which we are interested on evaluating Lagrangian chaos. For nonchaotic flow regimes λ_L is nonpositive, whereas for chaotic flow regimes λ_L is greater than zero. A more detailed description of the computational algorithms to calculate the Lagrangian trajectories from Eulerian velocity fields and the finite-time Lagrangian Lyapunov exponents can be found in Guzmán.[30]

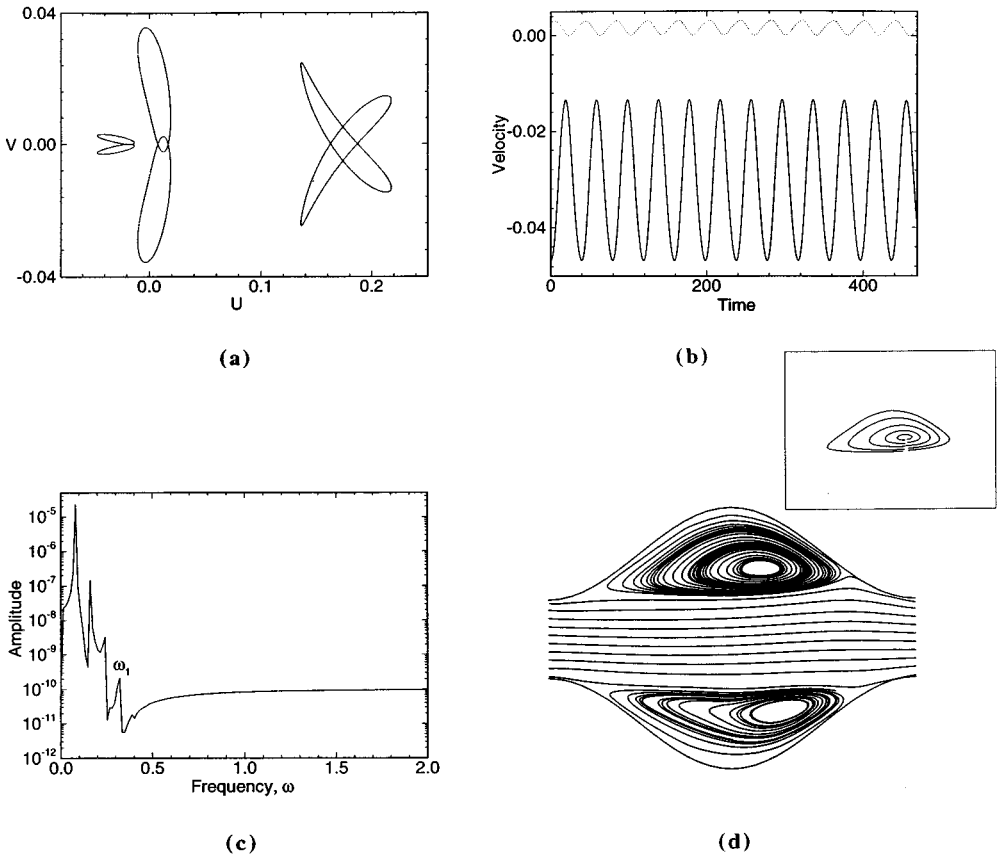

FIG. 3. Periodic flow regime for Re=150: (a) Phase-space trajectory of V vs U; (b) Streamwise U (solid line) and crosswise V (dotted line) velocities as a function of time; (c) Fourier power spectrum of the U velocity; and (d) instantaneous stream tracers.

V. RESULTS

In this section we present the computational simulations of laminar, transitional, and chaotic flow regimes, structured as follows: In Sec. V A, we discuss the Eulerian classical characterization of transitional and chaotic flow regimes in terms of phase portraits, velocity time series, Fourier power spectra, and instantaneous stream tracers; In Sec. V B, we present the Eulerian dynamical characterization of transitional and chaotic flow regimes in terms of Poincaré sections and Eulerian Lyapunov exponents. Last, in Sec. V C, we describe the Lagrangian characterization for these flow regimes based on Lagrangian trajectories and finite-time Lagrangian Lyapunov exponents.

A. Eulerian classical characterization

In this section we summarize the supercritical flow patterns predicted numerically as the Reynolds number is increased from 150 to 750. A self-sustained periodic oscillatory flow is obtained for Re=150, as shown in Fig. 3. This flow has evolved from a steady state to a limit cycle or periodic attractor by a first Hopf bifurcation. Figure 3(a) shows phase-space portraits of V crosswise velocity versus U streamwise velocity depicting the limit cycles at characteristic points located symmetrically in the channel (Fig. 1). Figure 3(b) shows the time evolution of the U and V velocities at a characteristic point of the flow domain. Both velocity components are impelled at the same frequency ω_1, except for points located at the central line of the channel, for which the ratio of the fundamental frequencies associated to the x- and y-flow directions, ω_x/ω_y, is 2 due to the symmetry of the channel.[25] The semilogarithmic Fourier power spectrum shown in Fig. 3(c) exhibits several peaks corresponding to the fundamental frequency $\omega_1=0.321\,651$ and its subharmonics. The Fourier spectrum of this supercritical flow confirms that the flow has experienced a bifurcation from a time-independent steady state to a time-dependent periodic flow. The smoothness of the traveling wave structure and the large-scale asymmetric vortices are shown in the instantaneous stream tracers of Fig. 3(d). A stream trace is the path traced out by a hypothetical massless particle placed in the *instantaneous* velocity field and it is calculated using a predictor–corrector integration algorithm.

As the Reynolds number is further increased ($200<\mathrm{Re}<500$), another flow instability occurs leading to a second supercritical Hopf bifurcation. An additional fundamental frequency ω_2 appears, which represents a quasiperiodic flow regime with two fundamental frequencies ω_1 and ω_2 and their linear combinations. A plot of the ω_1/ω_2 ratio and the fundamental frequencies ω_1 and ω_2 versus the Reynolds number is shown in Fig. 4. The ω_1/ω_2 ratio is, in general, an irrational number, indicating that both frequencies are incommensurate. In addition, this frequency ratio decreases as

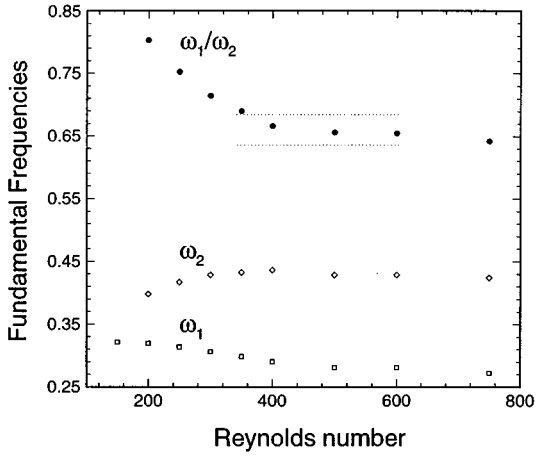

FIG. 4. Fundamental frequencies as a function of the Reynolds number.

the Reynolds number is increased until reaching asymptotically a plateau that coincides with the appearance of a frequency-locking phenomenon at Re=400. Similar frequency-locking phenomena have also been reported by Gollub and Benson[31] in Rayleigh–Bénard convective flows and, recently, by Vittori and Blondeaux[32] for a two-dimensional oscillatory flow around a circular cylinder. However, in those cases, further increases in the control parameters lead to chaotic flow regimes, whereas in the converging–diverging channel flow, a third supercritical Hopf bifurcation occurs for a higher Reynolds number (Re $\approx$500), leading to a quasiperiodic attractor with three fundamental frequencies and their linear combinations.[25]

Figure 5 presents the asymptotically converged, time-dependent flow regime corresponding to the frequency-locking phenomenon at Re=400. This flow regime is obtained by increasing the flow rate from a previous quasiperiodic flow with two incommensurate fundamental frequencies. The periodic flow behavior is clearly depicted by the closed curve in the phase-space portrait representing a limit cycle [Fig. 5(a)], and by the periodic velocity signals composed by ten complete periods τ of oscillations (τ =43.04) [Fig. 5(b)]. The Fourier power spectrum displays the locked fundamental frequencies ω_1 and ω_2, and a sequence of successive peaks corresponding to their harmonics. Finally, the instantaneous stream tracers [Fig. 5(d)] show the traveling wave structure and the complexity of motion with the coexistence of different scale vortices occupying both furrows of the channel.

In Fig. 6 the global flow structure is shown for Re=450 through a sequence of six time frames of instantaneous stream tracers for a period of time corresponding to the first fundamental frequency ω_1 of this self-sustained oscillatory flow. We notice the evolving complex topology of the vortex

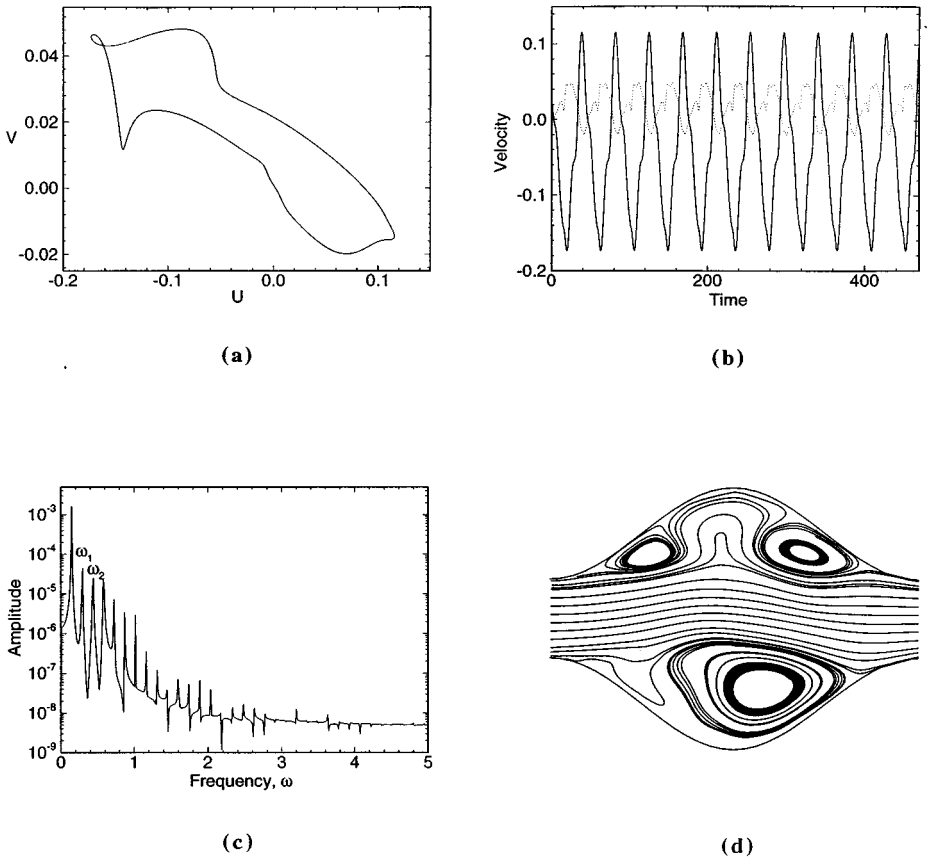

FIG. 5. Frequency-locking flow regime for Re=400: (a) Phase-space trajectory of V vs U; (b) streamwise U (solid line) and crosswise V (dotted line) velocities as a function of time; (c) Fourier power spectrum of the U velocity; and, (d) instantaneous stream tracers.

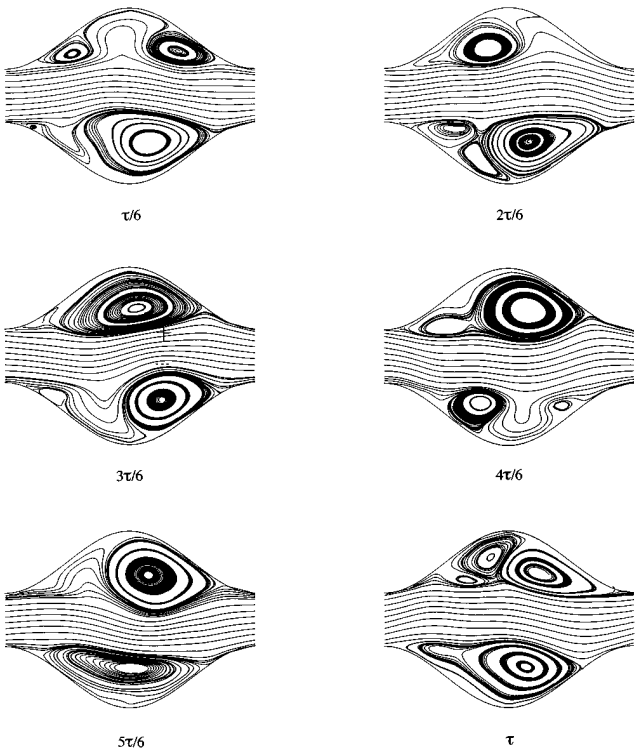

FIG. 6. Instantaneous stream tracers during one period of self-sustained oscillatory flow for Re=450 in a sequence of six time frames.

dynamics in the furrows with vortices bulging alternatively to the main flow stream.

An aperiodic flow behavior is obtained for Re=750 and shown in Fig. 7. The phase-space portrait and the time evolution of the velocity components indicate a seemingly random, but deterministic, chaotic motion. The large-scale variations of velocity in the chaotic time series are essentially similar to those in the quasiperiodic flow regime, except for a greatly increased number of small-scale fluctuations in the aperiodic regime. The Fourier power spectrum indicates that the peaks previously observed for Re=400 decrease in amplitude and tend to disappear into the background of a broadband continuous spectrum. However, there are still prevailing frequency peaks on the continuous spectrum. The instantaneous stream tracer plots for this Reynolds number depict large-scale vortices, also present in the previous flow regimes, coexisting with small-scale vortices, originated in this chaotic motion.

B. Eulerian dynamical characterization

The results from the Eulerian dynamical flow characterization are presented in terms of Poincaré sections and Eulerian Lyapunov exponents. Additional dynamical system parameters such as autocorrelation functions, pseudo-phase

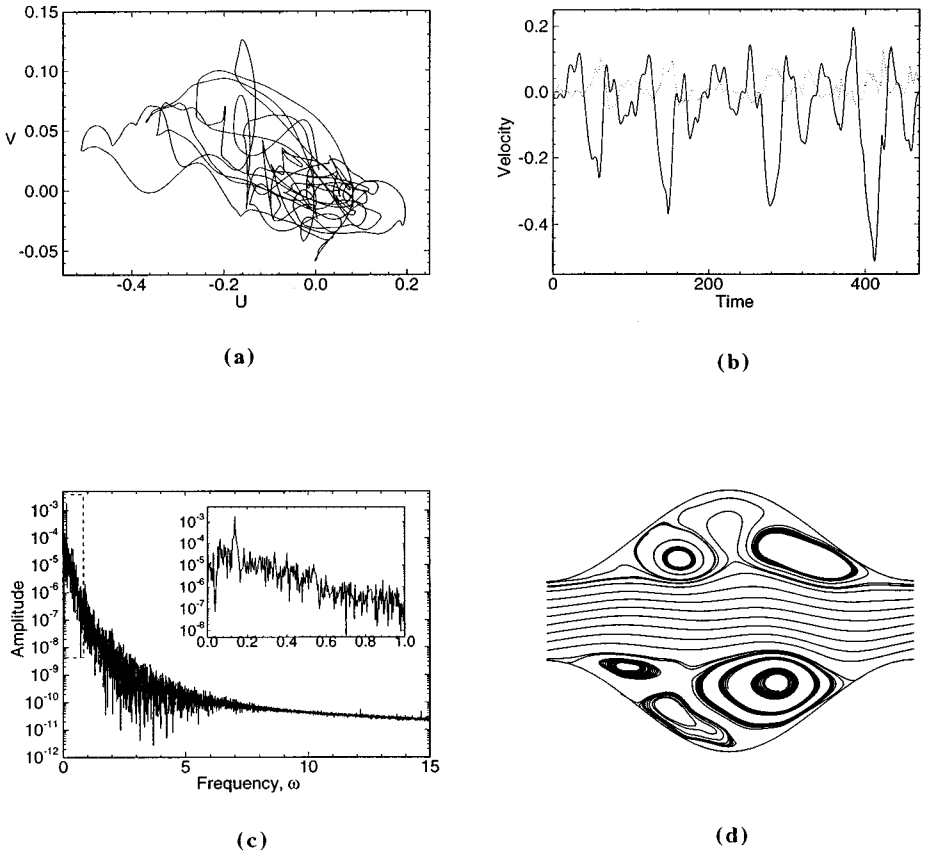

FIG. 7. Aperiodic flow regime for Re=750: (a) Phase-space trajectory of V vs U; (b) Streamwise U (solid line) and crosswise V (dotted line) velocities as a function of time; (c) Fourier power spectrum of the U velocity; and (d) instantaneous stream tracers.

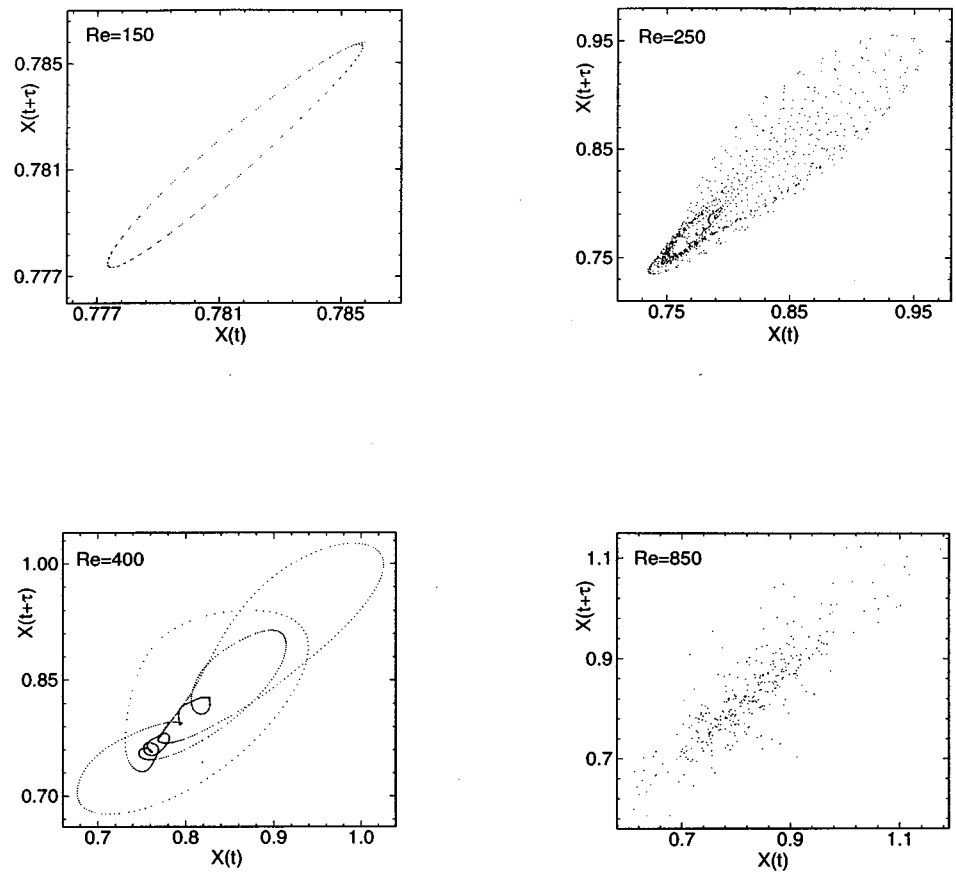

FIG. 8. Poincaré sections for Reynolds number range of 150–850.

space representations and fractal dimensions that verify the unpredictable nature of deterministic chaotic flow regimes are reported in Guzmán and Amon.[33]

1. Poincaré sections

Poincaré sections corresponding to continuous-time evolutions, for the Reynolds number range of 150 and 850, are shown in Fig. 8. The U-streamwise velocity component of the point indicated as 1 in Fig. 1 is used to construct the state vector. The time delay τ, for all the reconstructions, is 16 times the sampling nondimensional time, $\tau=0.375\,12$, and the nondimensional period T is 19.53. Very long computational simulations are performed to obtain accurate Poincaré section representations. We observe that well-organized structures exist for Reynolds number of 150, 250, and 400. For Re=150, points of the Poincaré section are located along a closed orbit, indicating the periodic nature of this flow regime. For the Reynolds number of 250, the Poincaré section shows that the orbits lie on a quasiperiodic T^2 torus. Because the ω_1/ω_2 ratio between fundamental frequencies is an irrational number, the trajectories in the phase space never close on themselves. The Poincaré section in this case is not a simple curve, but is rather distributed on a surface due to the presence of many harmonic combinations of ω_1 and of ω_2. For the Reynolds numbers of 400, the Poincaré section shows that the attractor is composed of several points in a closed curve, which indicates the periodic nature of this flow and the complicated shape of the limit cycle on the phase space. Moreover, the Poincaré section shows the frequency-locking phenomenon, already indicated in Sec. V A, occurring at this Reynolds number, and indicates how a quasiperiodic flow evolves to a periodic flow with many harmonics at a specific value of the ratio ω_1/ω_2. Last, for the Reynolds number of 850, the Poincaré section depicts a diffuse configuration of interception points. We have demonstrated previously[25] the existence of a quasiperiodic flow with three fundamental frequencies at Re=500 and an aperiodic flow regime at Re=850 represented by a broadband Fourier power spectrum. Consequently, the Poincaré section for Re =850 corresponds to a two-dimensional representation of a strange attractor.[33]

2. Eulerian Lyapunov exponents

Several techniques have been proposed to calculate Lyapunov exponents.[34–39] We use the algorithm described by Wolf *et al.*[34] to calculate the largest Eulerian Lyapunov exponent, λ_E, for a Reynolds number range between 150 and 850. This algorithm is appropriate for temporal evolutions of a signal and assumes no previous knowledge of the physics and of the attractor beyond the time series measurement.[34] Time series of 10 001 data points are used for all Reynolds numbers, except for Re=850 where 35 001 data points are used, and the embedding dimension for all the Reynolds numbers reported is $n=4$.[33] Figure 9 shows the temporal

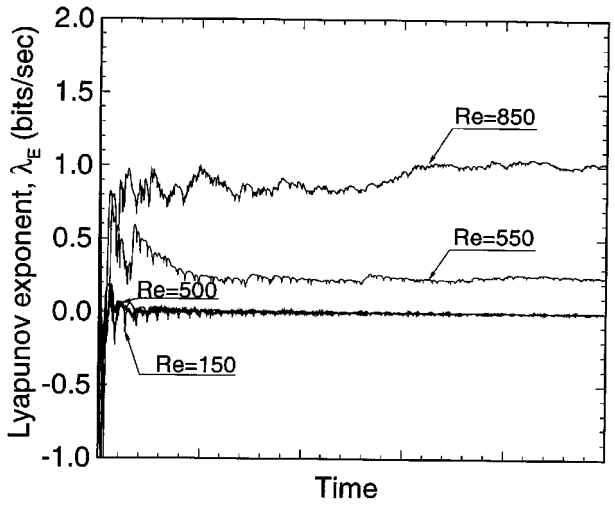

FIG. 9. Temporal convergence of the largest Eulerian Lyapunov exponent λ_E.

convergence of λ_E, which is the long-time average exponential growth or decay rate, for different Reynolds numbers. A zero value of the Eulerian Lyapunov exponent, λ_E, within acceptable numerical accuracy, is obtained for self-sustained periodic and quasiperiodic oscillatory flows up to Reynolds numbers of 500. These zero Eulerian Lyapunov exponents indicate that small perturbations in the initial conditions of the phase space decay exponentially toward the attractor. Positive Eulerian Lyapunov exponents, obtained for Reynolds numbers greater than 500, verify the chaotic flow behaviors.

The asymptotic values of the Eulerian Lyapunov exponents as a function of the Reynolds number are shown in Fig. 10. Periodic, quasiperiodic, and frequency-locking flow regimes have zero Eulerian Lyapunov exponents, whereas aperiodic chaotic flow regimes exhibit positive Eulerian Lyapunov exponents. The Eulerian Lyapunov exponent is definitely positive and remains almost constant around the value 1.1 for converging–diverging channel flows at

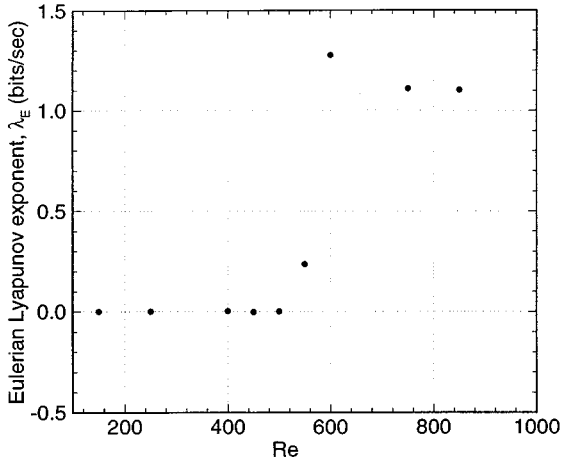

FIG. 10. Largest Eulerian Lyapunov exponent λ_E as a function of the Reynolds number.

Re$\geqslant$750. Other flow systems such as open unforced compressible flows past airfoils depict an increase in the Eulerian Lyapunov exponent as the Reynolds number is increased after the onset of chaos.[40]

C. Lagrangian characterization of laminar and transitional flo regimes

The results presented in previous sections demonstrate that the flow evolves from a well-organized velocity field to a regime of Eulerian chaos as the Reynolds number is increased. The positive Eulerian Lyapunov exponents, λ_E, for Reynolds number higher than 550 indicate chaotic flow regimes that are visualized by the Poincaré section representations. In this section, we present results for the Lagrangian descriptions of converging–diverging channel flows, in terms of test particle trajectories and spatial distribution of the finite-time Lagrangian Lyapunov exponents, λ_L. We describe Lagrangian trajectories for single test particles located throughout the flow and for pairs of test particles located in the vortex region. Then, we present the spatial distribution of the finite-time Lagrangian Lyapunov exponent, which enables us to measure the extension of chaotic regions, the strength of Lagrangian chaotic regimes, and the mixing enhancement due to chaotic advection.

1. Lagrangian trajectories of test particles

Figure 11 shows Lagrangian trajectories of three single test particles, initially located in different regions of the computational domain, for Reynolds numbers 125, 150, and 400, passing through many furrows of the channel. For Re=125 each test particle follows the same path in each furrow of the fully developed channel [Fig. 11(a)]. This behavior is originated by the steady laminar flow regime and, consequently, test particle trajectories coincide with the streamlines of the Eulerian velocity field. As the Reynolds number increases to 150, the test particle trajectories do not follow the same path in each furrow, as shown in Fig. 11(b). The test particle initially located in the middle of the channel follows a trajectory that remains in the central region of the channel. A close-up of this region indicates that this particle trajectory is sinusoidal, and it is synchronized with the periodic nature of the Eulerian velocity field shown in Sec. V A. The trajectory of a test particle, initially located in the vortex region, is trapped by the vortex dynamics for a finite amount of time before being ejected into the main flow. When the Reynolds number increases to 400, the particle trajectories become more complex, as shown in Fig. 11(c). A typical test particle that starts its motion in the middle of the channel continues to the vortex region and, finally, returns to the bulk flow. Similar complex trajectories are observed in test particles starting their motion in other regions. The complexity of the test particle trajectories increases when the flow evolves from a laminar to a transitional regime. As we will see later, the motion of test particles following complex trajectories and the divergence of initially close trajectories contribute to mixing enhancement.

Lagrangian trajectories of five pairs of test particles initially located in the vortex region for various Reynolds numbers are shown in Fig. 12. The initial and final positions are

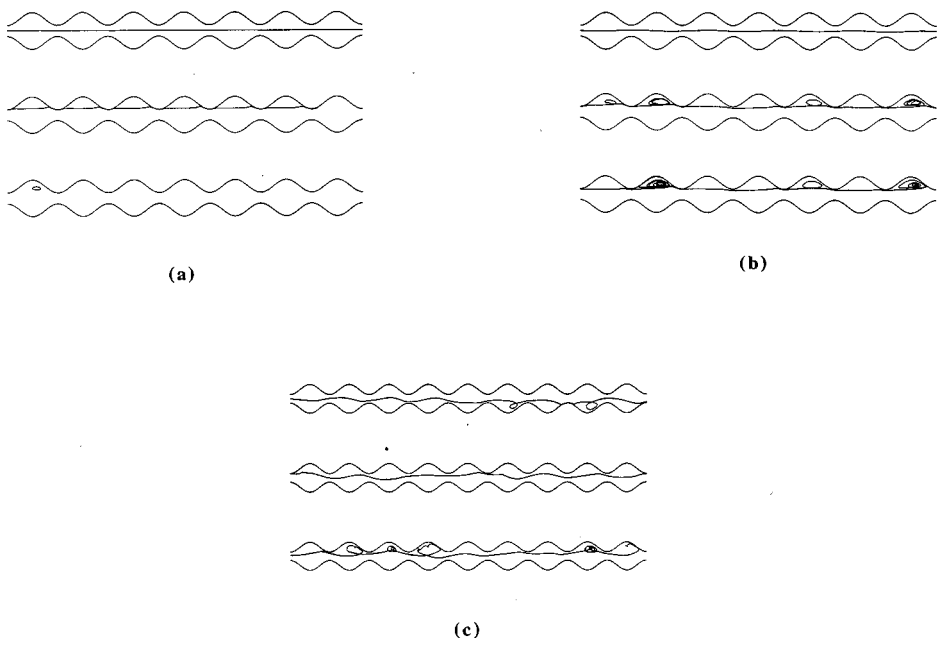

FIG. 11. Lagrangian trajectories of three single test particles: (a) Re=125; (b) Re=150; and (c) Re=400.

indicated by i and f, respectively. Each curve, composed of a sequence of points, represents the trajectories of one pair of test particles. The initial position of the test particles for all the Reynolds numbers is the same. The time for each trajectory to reach the final position depends on the initial position of the test particle in the velocity field. In addition, a pair of test particles at an initial position in a high-Reynolds number velocity field reaches its final position in less time than that required in a lower Reynolds number flow, because the velocity magnitude increases with the Reynolds number.

Figure 12(a) shows Lagrangian trajectories of five different test particles for Re=125, where the particles follow trajectories that coincide with the flow streamlines.[30] Moreover, test particles that begin their motion in the vortex region remain within it forever. A different pattern is observed when the Reynolds number increases to 150, where the trajectory of a pair of test particles remains in the vortex region but without repeating the same path [Fig. 12(b)]. This trajectory is synchronized with the oscillating motion of the vortices due to the periodic self-sustained flow regime described in Sec. V A. Figure 12(c) shows a more complex pattern of Lagrangian trajectories for Re=250. Some test particles remain in the vortex region, following complex trajectories before exiting the vortex region and, finally, the furrow. The complexity in trajectories increases even more at Re=600 for which some test particles exit the vortex region and the furrow immediately [Fig. 12(d)]. This pattern, originated by the complex dynamic of the different scale vortices interacting in the furrows of the channel, corresponds to the aperiodic Eulerian chaotic regime described in Secs. V A and V B.

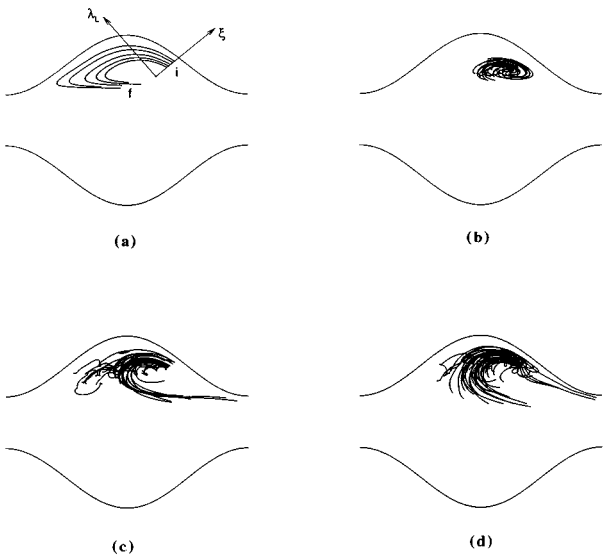

FIG. 12. Lagrangian trajectories of five pairs of test particles: (a) Re=125; (b) Re=150; (c) Re=250; and (d) Re=600.

With the purpose of determining whether Lagrangian chaos spreads to other flow regions as the Reynolds number increases, we consider Lagrangian trajectories of 13 pairs of test particles located initially in different regions of the channel. The initial positions of these test particles and small portions of their trajectories are depicted in Fig. 13(a) for Re=257. Four pairs of test particles are in the central region and nine pairs are in the lower furrow of the channel. Figure 13(b) shows that test particles initially located in the vortex region follow a pattern of Lagrangian trajectories similar to that of Re=250, whereas test particles initially located in the channel central region convect downstream with the quasiperiodic Eulerian velocity field.

The chaotic nature of particle trajectories, and the spreading of chaotic flow regimes to other regions, cannot be determined by simply looking at the particle paths, even

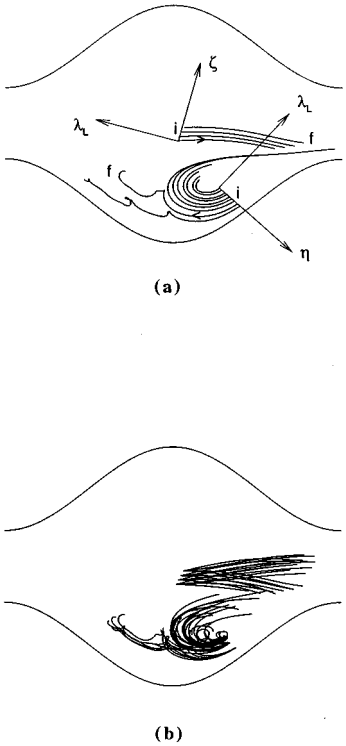

FIG. 13. Lagrangian trajectories of 13 pairs of test particles for Re=257: (a) Initial and final positions, i and f, respectively, of pairs of test particles after $\Delta t = t_i - t_0$; and (b) initial and final positions of fluid particle trajectories for long-time evolutions.

though complex paths could provide qualitative indications of chaos. Thus, we evaluate the divergence of trajectories of particles initially close by calculating the finite-time Lagrangian Lyapunov exponent, λ_L.

2. Finite-time Lagrangian Lyapunov exponents

Figure 14 shows the spatial distribution of finite-time Lagrangian Lyapunov exponents, λ_L, of pairs of test particles for Reynolds numbers equal to 150, 257, and 600. Three local coordinate systems are defined in Fig. 14(a) to represent the relative position of each pair of test particles. The $\lambda_L - \xi$ coordinate system is defined for test particles initially located in the vortex region of the upper furrow; the $\lambda_L - \zeta$ coordinate system is defined for test particles with initial positions in the channel central region; and the $\lambda_L - \eta$ coordinate system is defined for test particles initially located in the lower furrow vortex region.

The spatial distribution of λ_L for Reynolds numbers of 150 and 600 is shown in Fig. 14(b). The positive value of λ_L for the ten pairs of test particles, at both Reynolds numbers, indicates that there is a zone in the vortex region where trajectories of initially close particles diverge exponentially fast. This time-average divergence is uniformly distributed for Re=150, with a value of λ_L in the range 0.01–0.06, whereas for Re=600 is consistently higher as well as the spatial distribution of the finite-time Lagrangian Lyapunov exponent λ_L presents the highest values near the channel wall. The higher value of λ_L for Re=600 indicates that the

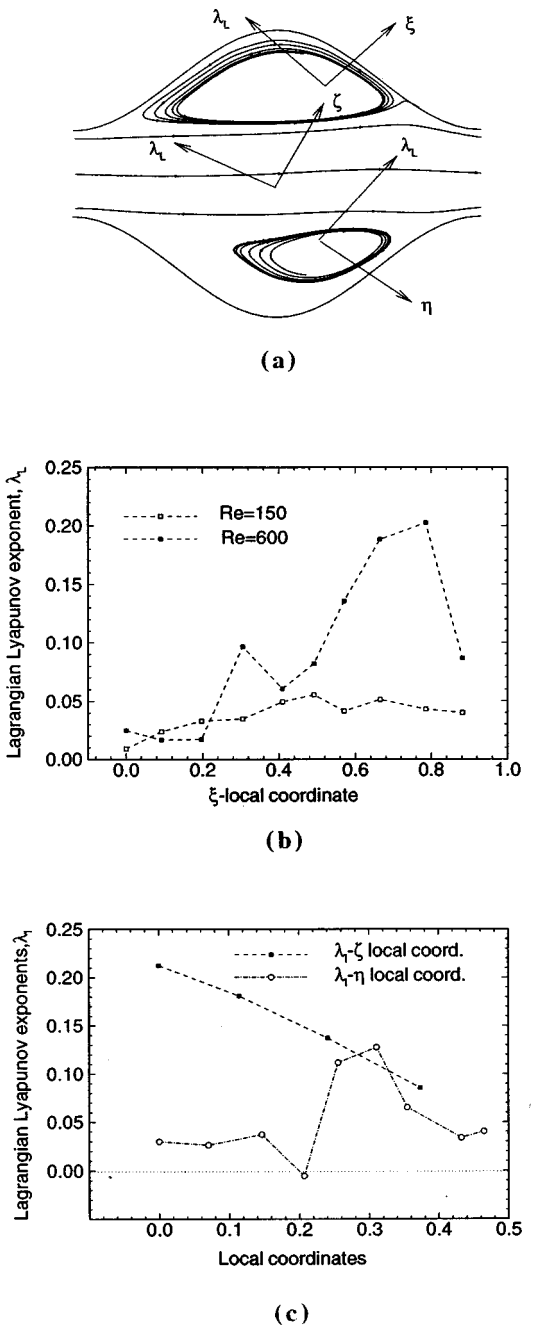

FIG. 14. Spatial distribution of finite-time Lagrangian Lyapunov exponents λ_L; (a) local coordinate systems; (b) Re=150 and 600; and (c) Re=257.

Lagrangian chaos regime becomes stronger as the flow regime approaches the onset of Eulerian chaos at Re≈550.

Figure 14(c) shows the spatial distribution of the finite-time Lagrangian Lyapunov exponents of test particles initially located in the central region and lower furrow vortex region for Re=257. The positive λ_L value for test particles located initially in the central region indicates that this flow region develops a strong regime of Lagrangian chaos. The spatial distribution of λ_L, for test particles initially located in the vortex region, is not uniform and positive values of λ_L can come from test particles located close to test particles with small negative values of λ_L. A negative λ_L value means that, on average, the initial distance between two initially

close fluid particles decreases with time. The varying spatial distribution of λ_L with negative and positive values shows that Lagrangian chaos has a complicated distribution and coexists with other zones where the flow is nonchaotic. It also demonstrates that Lagrangian chaos has partially spread to the whole domain.

VI. DISCUSSION

A. Eulerian flo characterization

Based on classical fluid dynamics representations, this investigation has revealed the possibility of triggering self-sustained oscillatory flows, has identified the Reynolds number range for periodic, quasiperiodic and aperiodic chaotic flow regimes, and has demonstrated that the route of transition to a chaotic flow regime occurs by successive supercritical Hopf bifurcations.

The transitional flow behavior is analyzed by the geometric visualization of the evolution of the attractors until the appearance of a strange attractor. The Poincaré section representations of the reconstructed attractors reveal the existence of a periodic flow attractor that evolves to a well-defined, T^2 torus, quasiperiodic attractor, and, then, to a periodic attractor corresponding to a frequency-locking flow regime as the Reynolds number is increased from 150 to 400. In this Reynolds number range, the well-organized structure of the flow trajectories confirms the predictability of these flow regimes. The evolution to a strange attractor for higher Reynolds numbers (e.g., Re=850) from previous quasiperiodic attractors establishes the unpredictable nature of the aperiodic orbits, as well as the emergence of a chaotic flow behavior via a sequence of successive supercritical bifurcations, as described in Guzmán and Amon.[25] The gradual transition to chaos through a sequence of bifurcations is also confirmed by the evolution of the values of the largest Eulerian Lyapunov exponent, λ_E, as the Reynolds number is increased. Vanishing Eulerian Lyapunov exponents correspond to periodic and quasiperiodic flow regimes, whereas, Eulerian Lyapunov exponents greater than zero represent chaotic flow regimes. The positive value of the largest, long-time average, Eulerian Lyapunov exponent, λ_E, indicates that chaotic flow regimes exist for $Re \geqslant 550$.

B. Lagrangian flo characterization

The Lagrangian characterization enables the determination of flow regions and flow regimes where Lagrangian chaos is present and can be exploited with the objective of improving mixing by chaotic advection. Lagrangian trajectories provide qualitative indications of the paths followed by fluid particles, whereas finite-time Lagrangian Lyapunov exponents provide quantitative evidence of the onset of Lagrangian chaos, the spreading of Lagrangian chaos to other flow regions, and the persistence and strength of Lagrangian chaotic regimes.

Lagrangian trajectories and finite-time Lagrangian Lyapunov exponents indicate that a weak Lagrangian chaotic regime is attained for low Reynolds numbers (e.g., Re=125 and 150), whereas stronger chaotic regimes are obtained for higher Reynolds numbers (e.g., Re=250, 257, and 600). We have shown that the trajectories followed by test particles increase in complexity when the flow evolves from a laminar to a transitional regime. Calculations of the finite-time Lagrangian Lyapunov exponent have indicated that a weak Lagrangian chaotic regime starts as a local phenomenon in the vortical regions of the fluid domain. The Lagrangian chaotic regime becomes stronger and spreads to other regions as the Reynolds number is further increased. For example, a pair of test particles located at the channel entrance at Re=125 presents a vanishing λ_L value that becomes positive at Re=250. Results also show that certain flow regions of the channel have negative or zero finite-time Lagrangian Lyapunov exponents (e.g., Re=257) and coexist with regions of Lagrangian chaos with strong positive λ_L values. Last, our results of λ_L for Re=600 demonstrate the existence of a strong Lagrangian chaotic regime in the vortex region, which extends over larger areas as the Reynolds number increases.

The laminar and chaotic mixing phenomena have been qualitatively visualized and quantitatively measured. By using Lagrangian trajectory representations, we have shown that a more complex pattern of Lagrangian trajectories is associated with a better mixing and that chaotic mixing, due to Lagrangian chaos, produces mixing enhancement. The efficiency of mixing is determined by the stretching rate which corresponds to the finite-time Lagrangian Lyapunov exponent. According to Ottino,[15] the stretching distribution can be interpreted as the finite-time Lagrangian Lyapunov exponent distribution. Based on calculations of λ_L, we can assert that the mixing effectiveness improves as the Reynolds number increases and the stretching rate increases as well.

Our calculations of Lagrangian and Eulerian Lyapunov exponents indicate that Lagrangian chaos exists in nonchaotic Eulerian velocity fields in the converging–diverging channel for the Reynolds number range between 150 and 450. We have found that the onset of Lagrangian chaos, at approximately Re=125, coincides with the appearance of the first Hopf bifurcation, as shown in Secs. V A and V C. This Hopf bifurcation represents the evolution from an initially steady flow to a stable limit cycle of periodic orbits. Our numerical results show no evidence of Lagrangian chaos for steady-state flow regimes, which is in agreement with the theoretical argument that time-independent two-dimensional flows do not present chaotic behavior.[17] They also indicate a Lagrangian chaotic behavior for the periodic, time-dependent, flow regime resulting from the first Hopf bifurcation. Therefore, we can assert that the onset of Lagrangian chaotic coincides with the appearance of the first Hopf bifurcation in the Eulerian flow representation.

In summary, we have found that (i) both Lagrangian and Eulerian Lyapunov exponents are positive for Re>550; (ii) regions of strong Lagrangian chaos exist for Re>250; and (iii) the onset of Eulerian chaos coincides with the spreading of Lagrangian chaos to the whole domain without producing an inverse effect on the positive λ_L. When Eulerian chaos sets in, regions of Lagrangian chaos remain chaotic, and regions with previously weak positive and vanishing λ_L values become chaotic. Therefore, the onset of Eulerian chaos does not have a reversing effect on the Lagrangian chaotic flow behavior. Moreover, a chaotic velocity field implies chaotic

motions of fluid particles in converging–diverging channel flows. This finding also agrees with most cases studied to date, with the exception of the point vortex model[5] and the Lorenz model,[7] where Eulerian chaos does not imply Lagrangian chaos and, in which, two nearby particles remain close during their evolution in a chaotic Eulerian velocity field.[3–5,7]

VII. CONCLUSIONS

Direct numerical simulations of the governing flow equations enable the characterization of converging–diverging channel flows in terms of classical fluid dynamic representations, Eulerian dynamical characterizations, and Lagrangian flow characterizations. The Eulerian dynamical characterization of the reconstructed attractors confirms that the periodic flow attractor evolves to a well-defined, T^2 torus, quasiperiodic attractor and, then, to a periodic, frequency-locking flow attractor as the Reynolds number is increased from 150 to 400. The quasiperiodic T^2 torus leads to a T^3 torus, which breaks up into a chaotic strange attractor at $500<\mathrm{Re}<550$. The gradual evolution to a strange attractor from previous quasiperiodic and periodic attractors establishes the emergence of an Eulerian chaotic flow via successive bifurcations of transitional flows.

The dynamical flow characterization of the transitional flow regimes ascertains the Reynolds number range for the onset of Eulerian chaos. The value of the largest Eulerian Lyapunov exponent verifies the change of flow behavior from a quasiperiodic predictable regime to an aperiodic, chaotic, unpredictable regime in the Reynolds number range between 500 and 550. For predictable flows in the periodic, quasiperiodic and frequency-locking regimes, the Eulerian Lyapunov exponents are zero, which indicate the insensitivity to initial conditions and the exponential decay toward the attractor. For higher Reynolds numbers, $550\leqslant\mathrm{Re}\leqslant850$, the flow remains chaotic, as verified by the largest positive Eulerian Lyapunov exponent.

The onset of Lagrangian chaos at $125<\mathrm{Re}<150$ coincides with the first Hopf bifurcation to Eulerian time-dependent flows. Lagrangian trajectories and finite-time Lagrangian Lyapunov exponents identify (i) weak Lagrangian chaos localized in the vortical regions for low Reynolds number flows (e.g., $\mathrm{Re}=125$, 150); (ii) Lagrangian chaotic regions that spread to other flow regions of the converging–diverging channel as the Reynolds number is increased; (iii) the coexistence of nonchaotic and chaotic flow regions at $\mathrm{Re}=257$; and (iv) the emergence of a strong generalized Lagrangian chaotic regime at $\mathrm{Re}>550$, which coincides with the onset of Eulerian chaos.

Lagrangian trajectories of test particles increase in complexity as the flow evolves through transitional regimes. Complex trajectories in Lagrangian chaos induce chaotic advection, which, in turn, produces mixing enhancement further verified by positive finite-time Lagrangian Lyapunov exponents and stretching rate distributions. Lagrangian and Eulerian Lyapunov exponents assert that Lagrangian chaos exists in nonchaotic Eulerian velocity fields for $125<\mathrm{Re}<550$, and chaotic velocity fields are accompanied by chaotic trajectories of all fluid particles for $\mathrm{Re}>550$ in converging–diverging channel flows.

ACKNOWLEDGMENTS

Support by the Chilean MIDEPLAN Scholarship, National Science Foundation Grant No. CTS-9311072, Pittsburgh Supercomputer Center, and University of Pittsburgh Medical Center is gratefully acknowledged.

[1] J. M. Ottino, ''New applications of chaos in chemical engineering: Intuition versus prediction,'' in *Applied Chaos*, edited by J. H. Kim and J. Stringer (Wiley, New York 1992).
[2] J. P. Eckmann and D. Ruelle, ''Ergodic theory of chaos and strange attractors,'' Rev. Mod. Phys. **57**, 617 (1985).
[3] T. J. Danielson and J. M. Ottino, ''Structural stability in two-dimensional model flows: Lagrangian and Eulerian turbulence,'' Phys. Fluids A **2**, 2024 (1990).
[4] T. J. Crisanti, M. Falcioni, A. Vulpiani, and G. Paladin, ''Lagrangian chaos: Transport, mixing and diffusion in fluids,'' Riv. Nuovo Cimento **14**, 1 (1991).
[5] A. Babiano, G. Boffetta, A. Provenzale, and A. Vulpiani, ''Chaotic advection in point vortex models and two-dimensional turbulence,'' Phys. Fluids **6**, 2465 (1994).
[6] V. Rom-Kedar, A. Leonard, and S. Wiggins, ''An analytical study of transport, mixing, and chaos in an unsteady vortical flow,'' J. Fluid Mech. **214**, 347 (1990).
[7] E. N. Lorenz, ''Deterministic nonperiodic flow,'' J. Atmos. Sci. **20**, 30 (1963).
[8] H. Aref, ''Stirring by chaotic advection,'' J. Fluid Mech. **143**, 1 (1984).
[9] I. J. Sobey, ''Dispersion caused by separation during oscillatory flow through a furrowed channel,'' Chem. Eng. Sci. **40**, 2129 (1985).
[10] J. Chaiken, R. Chevray, M. Tabor, and Q. M. Tan, ''Experimental study of Lagrangian turbulence in Stokes flows,'' Proc. R. Soc. London Ser. A **408**, 105 (1986).
[11] W.-L. Chien, H. Rising, and J. M. Ottino, ''Laminar and chaotic mixing in several cavity flows,'' J. Fluid Mech. **170**, 355 (1986).
[12] T. Howes, M. R. Mackley, and E. P. L. Roberts, ''The simulation of chaotic mixing and dispersion for periodic flows in baffled channels,'' Chem. Eng. Sci. **46**, 1669 (1991).
[13] J. S. Perkins, K. D. Stephanoff, and B. T. Murray, ''Mixing enhancement in flow past rectangular cavities as a result of periodically pulsed fluid motion,'' *Proceedings of the 5th Annual IEEE Semiconductor Thermal and Temperature Measurement Symposium* (1989), p. 93.
[14] A. V. Tangborn and V. Lakshminarayanan, ''A three-dimensional instability in mixed convection with streamwise periodic heating'' (private communication, 1994).
[15] T. H. Solomon and J. P. Gollub, ''Chaotic particle transport in time-dependent Rayleigh–Bénard convection,'' Phys. Rev. A **38**, 6280 (1988).
[16] K. Shariff, T. H. Pulliam, and J. M. Ottino, ''A dynamical system analysis of kinematics in the time-periodic wake of a circular cylinder,'' in *Vortex Dynamics and Vortex Methods* (1992), p. 613.
[17] J. M. Ottino, *The Kinematics of Mixing: Stretching, Chaos, and Transport* (Cambridge University Press, Cambridge, 1989).
[18] H. Aref, ''Stochastic particle motion in laminar flows,'' Phys. Fluids A **3**, 1009 (1991).
[19] I. J. Sobey, ''On flow through furrowed channels. Part 1. Calculated flow patterns,'' J. Fluid Mech. **96**, 1 (1980).
[20] E. M. Sparrow and A. T. Prata, ''Numerical solutions for laminar flow and heat transfer in a periodically converging–diverging tube with experimental confirmation,'' Num. Heat Transfer **6**, 441 (1983).
[21] M. E. Ralph, ''Oscillatory flows in wavy-walled tubes,'' J. Fluid Mech. **168**, 515 (1986).
[22] V. K. Gargand and P. K. Maji, ''Laminar flow and heat transfer in a periodically converging–diverging pipe,'' *1987 ASME National Heat Transfer Conference*, Pittsburgh, PA, ASME-HT **26**, 1 (1987).
[23] T. Nishimura, S. Murakami, S. Arakawa, and Y. Kawamura, ''Flow observations and mass transfer characteristics in symmetrical wavy-walled channels at moderate Reynolds number for steady flow,'' Int. J. Heat Mass Transfer **33**, 835 (1990).
[24] M. Faghri and Y. Asako, ''Numerical determination of heat transfer and

pressure drop characteristics for a converging–diverging flow channel,'' ASME J. Heat Transfer **109**, 606 (1987).
[25]A. M. Guzmán and C. H. Amon, ''Transition to chaos in converging–diverging channel flows: Ruelle–Takens–Newhouse scenario,'' Phys. Fluids A **6**, 1994 (1994).
[26]A. T. Patera, ''A Spectral element method for fluid dynamics: Laminar flow in a channel expansion,'' J. Comput. Phys. **54**, 468 (1984).
[27]C. H. Amon, ''Spectral element–Fourier method for transitional flows in complex geometries,'' AIAA J. **31**, 42 (1993).
[28]P. Bergé, Y. Pomeau, and C. Vidal, *Order Within Chaos* (Wiley, New York, 1986).
[29]F. Takens, ''Detecting strange attractors in turbulence,'' in *Dynamical Systems and Turbulence, Warwick 1980*, Lecture Notes in Mathematics (Springer-Verlag, New York, 1981), Vol. 898, p. 336.
[30]A. M. Guzmán, ''Lagrangian and Eulerian characterization of converging–diverging channel flows: Chaos, mixing, and heat transfer enhancement,'' Ph. D. thesis, Carnegie Mellon University, 1995.
[31]J. P. Gollub and S. H. Benson, ''Many routes to turbulent convection,'' J. Fluid Mech. **100**, 449 (1980).
[32]G. Vittori and P. Blondeaux, ''Quasiperiodicity and phase locking route to chaos in the 2-D oscillatory flow around a circular cylinder,'' Phys. Fluids A **5**, 1866 (1993).
[33]A. M. Guzmán and C. H. Amon, ''Dynamical flow characterization of transitional and chaotic regimes in converging–diverging channels,'' to appear in J. Fluid. Mech. (1996).
[34]A. Wolf, J. B. Swift, H. L. Swinney, and J. A. Vastano, ''Determining Lyapunov exponents from a time series,'' Physica D **16**, 285 (1985).
[35]J. P. Eckmann, S. O. Kamphorst, D. Ruelle, and S. Ciliberto, ''Liapunov exponents from time series,'' Phys. Review A **34**, 4971 (1986).
[36]K. Briggs, ''An improved method for estimating Liapunov exponents of chaotic time series,'' Phys. Lett. A **151**, 27 (1990).
[37]J. A. Vastano and R. D. Moser, ''Short-time Lyapunov exponent analysis and the transition to chaos in Taylor–Couette flow,'' J. Fluid. Mech. **233**, 83 (1991).
[38]M. Rosenstein, J. J. Collins, and C. J. De Luca, ''A practical method for calculating largest Lyapunov exponents from small data sets,'' Physica D **65**, 117 (1993).
[39]G. Barna and I. Tsuda, ''A new method for computing Lyapunov exponents,'' Phys. Lett. A **175**, 421 (1993).
[40]T. H. Pulliam and J. A. Vastano, ''Transition to chaos in an open unforced 2D flow,'' J. Comput. Phys. **105**, 133 (1993).